Received 24 January 2024; revised 3 March 2024; accepted 9 March 2024. Date of publication 18 March 2024; date of current version 6 August 2024.

Digital Object Identifier 10.1109/OJAP.2024.3378116

Modeling of the Fault Detection Problem for a 3-D Hybrid Antenna Array: Analysis and Evaluation

SOMAYEH KOMEYLIAN AND CHRISTOPHER PAOLINI (Member, IEEE)

Department of Electrical and Computer Engineering, San Diego State University, San Diego, CA 92182, USA

CORRESPONDING AUTHOR: C. PAOLINI (e-mail: paolini@engineering.sdsu.edu)

This work was supported by the Office of Naval Research (ONR) under Award N00014-21-1-2023.

ABSTRACT Research in the field of fault detection has steadily been developing for monitoring the performance of array antennas in the presence of errors in excitation phases and amplitudes. The presence of faulty elements degrades significantly the radiation characteristics and performance of antenna arrays. The measured errors in excitation phases and amplitudes at outputs of elements of the 3D HAAwBE are characterized by a few sparse non-zero vectors. A regularized $l_{2,1}$-norm problem is designed to model errors of faulty elements and noise. In this work, we have implemented the ADMM method under the joint sparsity setting to solve the regularized $l_{2,1}$-norm problem for a number of samples of the degraded radiation pattern of the HAAwBE rather than computing its array factor, which requires significant and complex mathematical computation. The proposed ADMM technique under the joint sparsity setting allows for minimizing the cost function of the problem with respect to both model parameters and variable vectors. We have further increased accuracy and stability of the performance of the HAAwBE in the two problems of fault detection and DoA estimation by deploying three different optimization methods: LS-SVM, NN-RBF, and NN-MLP, and compared to each other. Consequently, the superior performance of the HAAwBE has been numerically verified by the high success rates of 91.83%, 91.24%, and 88.33%, by performing the LS-SVM, NN-MLP, and NN-RBF optimization methods, respectively, in the presence of 50% faulty elements. Furthermore, results of DoA estimation by the HAAwBE have represented the high resolution in recognizing locations of three signal sources with performing the optimization method.

INDEX TERMS Fault detection, neural networks, multilayer perceptron, radial basis function, least squares support vector machine, direction of arrival estimation, joint group sparsity, alternating direction method of multipliers.

I. INTRODUCTION

ARRAY signal processing techniques have been steadily advancing for potential applications in problems of DoA estimation, fault detection, beamforming, beamsteering and nullsteering, [1], [2], [3], [4], [5], [6], [7], [8], [9], [10], [11], [12], [13], [14], [15], [16], [17], [18], [19], [20], [21], [22], [23], [24], [25]. The question of how the performance of array antennas under test, and their involved optimization methods is degraded in the presence of faulty and non-radiating elements, is still a challenging issue in the array signal processing framework.

Insufficient and missing information (or zeros) in the measured raw data at outputs of 72 elements of our proposed Hybrid Antenna Array with Bowtie Elements (HAAwBE), which is also affected by noise, makes it practically hard to train and retrieve accurate inputs and signal sources. Element excitations in array antennas are generally degraded due to the presence of errors in their amplitudes and phases. Hence, any defects in phases and amplitudes of element excitations are characterized by errors and non-deterministic noise. Manufactured imperfections, short circuiting states in electronic devices, fabrication defects, and drifting temperature in practice provide errors in excitation amplitudes and yield zero amplitudes. Errors in excitation phases result from temporary deviations in the power system under test in two main scenarios: (1) mutual coupling and insertion loss, which are accompanied by the presence of errors in phases, and (2) a sudden increase in current and thereby shorted

circuits in the system under test. Hence, the maximum phases are somehow associated with the presence of radiating elements, which denote "ON". On the other hand, non-radiating elements are associated with minimum phases that allow for degrading the radiation pattern and causing "OFF" states. Consequently, we can categorize all errors in element excitations into two states: (1) partial errors, and (2) ON-OFF failures. van den Biggelaar et al. in [1] have verified that random errors of excitation amplitudes and phases are significantly correlated in practice, and array elements possess different radiation patterns. Hence, we have to design a model that includes variables of sparse representations of few non-zero vectors of measured radiation patterns resulting from all faulty and non-faulty elements of the HAAwBE.

Although authors in [2], [3] have shown the high success rates in recognizing faulty elements; however, massive and complex mathematical computations should be performed for estimating array factors of configurations of array antennas under test. The performance of the proposed algorithms degrades significantly when antenna arrays under test change to more complicated configurations of 3D, and additional evaluations are required to obtain accurate and valid results. However, in this work, the proposed model is trained with a limited number of samples of the degraded radiation pattern, which yields a substantial increase in the speed of computations and thereby faster recognition of faulty elements of the HAAwBE.

Our first aim is to define a mathematical framework for our problem, based on the regularized $l_{2,1}$-norm problem, as expressed in Eq. (1).

$$\min_{\tilde{x}\in\delta^{2K+1}} \frac{1}{2\mu} \underbrace{\left\|\tilde{R}-\tilde{A}\tilde{x}\right\|_2^2}_{\text{Data fidelity}} + \underbrace{\tau\|\tilde{x}\|_{\omega,2,1}}_{\text{Signal prior}} \tag{1}$$

The regularized $l_{2,1}$-norm problem provides several different advantages for problems of the group sparse reconstruction, such as a significant reduction in their errors, convex approximation, and robustness to noise. The regularizer, or $l_{2,1}$-norm, provides additional information about whether the proposed solution to estimate the vector of $\tilde{x}$ are feasible and plausible for applications of interest or not.

Sparse groups of the regularized $l_{w,2,1}$-norm problem overlap together. These dependencies are caused by the weak performance of sparsity for which all coefficients of excitation amplitudes and phases are sparsified by an isotropic decomposition. An alternative way to overcome this limitation consists of transforming the overlapping group sparsity regularized $l_{w,2,1}$-norm problem to its counterpart problem with non-overlapping group sparsity. The joint sparsity of phase and amplitude excitations of elements of the HAAwBE denotes a set of sparse vectors, with common supports. We have assigned these sparse vectors into rows of the solution matrix of $\tilde{A}$. Hence, this matrix includes few non-zero columns, which are not necessarily sparse.

Neural networks and other machine learning approaches such as Least Squares Support Vector Machine (LS-SVM) have been increasingly developed for the array signal processing by various research groups, [4], [5], [6]. In this work, we aim to develop two well-established neural networks including Radial Basis Function (RBF) [4] and Multilayer Perceptron (MLP) [5], compared with the LS-SVM technique [6], for solving the problem of Eq. (1). However, the available algorithms for training neural networks and LS-SVM are not ideal scenarios for hardware deployments. These algorithms consist of a significant sequential dependencies. In order to develop our proposed model such that it becomes more compatible for hardware acceleration, we have to utilize iterative methods of least squares and Euclidean distance to avoid matrix inversion computations during training.

Back propagation and gradient-based algorithms have been typically utilized for training neural networks. The main limitation of these neural networks consists of several matrix multiplications, which in some scenarios results in vanishing gradients and a consequent slowing down or stopping of the training procedure. In some other scenarios, many matrix multiplications of gradient values of neural network models would cause exploding gradients, which lead to an unstable training procedure. Another disadvantage of neural networks is their unscalable features, which result from the nature of their gradient-based algorithms and their sequential dependencies. Generally, these neural networks and LS-SVM models include non-convex and ill-conditioned problems.

Hence, to overcome all aforementioned restrictions, the three NN-MLP, NN-RBF, and LS-SVM models have been trained by the Alternating Direction Method of Multipliers (ADMM) technique with the joint group sparsity setting. We have expanded the ADMM technique into the primal and dual forms of the regularized $l_{2,1}$-norm problem and estimated closed form solutions for their sub-problems. The primal algorithm minimizes Eq. (1) with respect to the variable vector of x and z. However, the dual algorithm tries to minimize Eq. (1) with respect to the model parameter of y, which is accompanied by the supervised training procedure in the three proposed optimization techniques. The primal-based problem tries to minimize or maximize an objective function under a set of given constraints, while the dual-based problem allows for achieving a best set of constraints under the given conditions. The joint sparsity setting for the ADMM technique without non-overlapping groups allows for minimizing Eq. (1) with respect to both of the model parameter of y and variable vectors of x and z.

Consequently, we have implemented the three different optimization techniques to minimize errors between outputs of models and an ideal radiation pattern of the HAAwBE without any faulty elements. Indeed, mapping samples of the degraded radiation pattern of the HAAwBE to labels within the training procedure of the three different optimization techniques is performed by minimizing the cost function of Eq. (1).

The major contributions of this work are outlined as follows,

- We are the first authors to train the LS-SVM, NN-MLP, and NN-RBF models with the ADMM algorithm for DoA estimation and fault detection problems. Figure 5 shows the HAAwBE performance enhancement by deploying the LS-SVM optimization model. Table 10 reports all three optimization models yield success rates that exceed 88% in identifying the locations of faulty elements.
- Our proposed three-class classification LS-SVM model for the 3D HAAwBE with 72 elements has illustrated a very high resolution in recognizing locations of signal sources in the presence of 83% faulty elements. DoA estimation problems allow for retrieving directions of signal sources from impinging electromagnetic waves in elements of the hybrid antenna array. We have verified that without performing any optimization method, the HAAwBE is not capable of recognizing locations of sources in the presence of faulty elements. In this case, the plot of DoA estimation has just represented a periodic oscillation around its normalized expected mean value of 0.25. However, we have verified that with implementing the three-class classification LS-SVM model, the HAAwBE can recognize locations of three sources with high resolution [7].
- Effects of faulty elements on the performance of an HAAwBE have been evaluated. An increase in the number of non-radiating elements, which is accompanied by an increase in failure probability, yields a significant degradation in the radiation pattern, growth in sidelobe levels (SLLs), and a reduction in depths of nulls and shifts in nulls. Fault diagnosis optimization models bring the merit of detecting and classifying faulty elements by performing feature extraction and pattern classification. We have also verified that the HAAwBE effectiveness in the fault detection problem varies for the three optimizations models. The superiority of the HAAwBE performance with performing the NN-RBF, LS-SVM, and MLP optimization models has been respectively verified for *low*, *medium*, and *high* percentages of faulty elements. Moreover, the high success rates of 91.83%, 91.24%, and 88.23% of the three NN-RBF, NN-MLP, and LS-SVM models, respectively, can guarantee the superiority of the HAAwBE performance in discriminating radiating elements from non-radiating (faulty) elements with high resolution and accuracy in the presence of 50% faulty elements.

Finally, in addition to the introduction section, this work is organized into the four following sections: An outline and overview of the related studies is concisely presented in Section II. Section III is devoted to describe the methodology and background of the involved approaches and techniques. The HAAwBE performance, by performing the optimization models for fault detection and DoA estimation problems, is discussed in Section IV. In Section V, we present the main conclusions of this research study.

II. LITERATURE REVIEW OF RELATED STUDIES

Fault detection problems include several different practical implications and limitations, which were debated and discussed in detail in [1], [2], [3], [4], [5], [7], [8], [9], [10], [11], [12], [13], [14], [15], [16], [17], [18]. Each of these approaches and techniques has its own advantages and constraints. In order to further highlight the effectiveness and strength of our proposed methods for identifying faulty elements of the 3D HAAwBE, we aim to concisely overview some of the available techniques and methods of fault detection.

Techniques for near-field measurements for the fault detection problems have been developing by various research groups [19], [20]. The near-field measurements of the excitation of an antenna array were accomplished by an infinitesimal tip of a probe in [21]. van Rensburg and Nearfield in [21] have verified that small changes in excitation of the array vector can be detected by near-field measurements. However, any changes in magnitudes of the excitation of the antenna array may not be determined in the near field region [21]. Furthermore, antenna arrays have potential applications in Radars, and wireless communication channels, which are not accessible to individuals in near field regions. Hence, near-field measurements of antenna arrays become practically infeasible [19] in the aforementioned applications.

Harrou and Sun in [22] have employed the generalized likelihood ratio technique for overcoming the limitations of non-parametric maximum likelihood ratio techniques and other available methods in fault detection problems for the linear antenna array. The proposed method has been verified for only 16.16% of the total number of array elements, which is insufficient for assessing its performance. Moreover, the proposed method in [22] includes intensive computations with very slow rates of convergence [23].

Vakula and Sarma in [24] have extended the two optimization methods of RBF and probabilistic neural network (PNN) for the 5×5 planar antenna array to identify locations of 12% faulty elements of the total array elements. Amplitudes and phases of pattern deviations [24] degrade significantly by increasing the number of defective elements, implying more irregularities in the actual radiation patterns of the planar antenna array. This also represents the strong sensitivity of the antenna performance to the number of faulty elements, which can cause a substantial degradation in the performance of the fault detection problem for array elements by increasing the number of defective elements.

Boopalan et al. in [20] have verified that the performance of the PSO optimization method is highly affected by the arrangement of defective elements in the planar antenna array. Indeed, a PSO technique is associated with the successful performance of adjacent elements of the array

TABLE 1. Comparative table to highlight the innovation of this work.

Authors	Antenna Array Configuration	Methodological Techniques	Advantages	Disadvantages
[19]-[21]	Planar Antenna Array	Based on the near field measurements	Higher sampling density in the near field.	A high dependency of measurements to probe and infeasibility for wireless systems in practice.
[22] and [23]	Linear antenna arrays	Generalized likelihood ratio (GLR)	Effective to detect faulty elements	High computational complexity, slow rates of convergence. Assessment only for a low percentage of faulty elements (16.16%).
[24]	Planar Antenna array	Neural Networks	Able to diagnose ON-OFF faults	Based on intensive computation for obtaining array factor. Sensitive performance to the number of faulty elements.
[20]	Planar Antenna Array	Particle swarm optimization (PSO)	Able to detect faulty elements in the presence of small number of elements	Inefficient for an increase in the number of faulty elements. Based on intensive computation for obtaining array factor.
This work	First time for the 3D Hybrid antenna array	Implementation of the optimization models (NN-MLP, NN-RBF and LS-SVM) trained by the ADMM technique using limited samples of a degraded radiation pattern.	Highly effective for DoA estimation with high resolution in the percentage high faulty elements. Fault detection with high success rates. Independent to intensive computations of array factor for the 3D antenna array. Invariant performance to the percentage of faulty elements	N/A

antenna under test in [20] and [25]. Although they could rigorously determine locations of elements in the four different arrangements of 25% defective elements, including random, row, column, and group [20], an increase in the numbers of array elements can fail to convergence.

The presented algorithms for the fault detection problem in [3] are performed by estimating array factors of array antennas under test, which require time-consuming and complex computations. Although Rodriguez-Gonzalez et al. in [18] could significantly improve the performance and speed of the fault detection problem of the linear array antenna by processing only samples of the degraded radiation pattern, the equivalent success rates are not achievable for complex configurations of array antennas such as 3D array antennas. Hence, we have increased the computational speed and accuracy by representing a new framework of the regularized $l_{2,1}$-norm problem and implementing the ADMM reconstruction method for a limited numbers of samples of the degraded radiation pattern of the 3D HAAwBE with 72 elements. Moreover, to achieve invariance (with respect to variations in the initialization performance and numbers of defective elements) and accuracy in the fault detection problem, we have updated hyperparameters and variables of the ADMM technique within the training procedures of the three different optimization methods of the LS-SVM, NN-RBF, and NN-MLP compared to each other. Table 1 shows a comparative table to highlight the innovation of this work.

In the real environment, which requires a maximum rate of data processing and transfer, the time complexity of NN-RBF, NN-MLP, and LS-SVM is proportional to the input size and the number of real and complex multiplications and additions. The conventional neural networks and machine learning techniques have been implemented for problems of DoA estimation and fault detection in the linear array antennas [26], [27] and planar array antennas [28]. Moreover, the proposed techniques, [29], [30], [31], include computational complexity for estimating array factors in DoA estimation problems. The practical challenge of the complexity of the aforementioned techniques become more dominant in problems of DoA estimation and fault detection when configurations of antenna arrays become 3D and more complex, and the number of array elements increases. To address the practical challenge of the time complexity of neural networks and machine learning techniques, we have randomly selected 35 samples of the degraded radiation pattern rather than estimating the array factor. We also enhanced the parallel computing performance of NN-MLP, NN-RBF, and LS-SVM models using the ADMM rather than the existing training methods, to maximize the rate of processing and transferring data. In this work, we assumed

that the size of the training dataset and the testing dataset is equal to 56×67, and the given dataset has been randomly partitioned into 75% for training and 25% for testing.

III. METHODOLOGICAL TECHNIQUES AND APPROACHES

As discussed in the introduction, we have chosen a number of required samples of the degraded radiation pattern of the HAAwBE to solve the problem of Eq. (1), rather than involving substantial mathematical computations for estimating array factors of array antennas under test in the existing technical literature [32], [33]. We have verified that a number of required samples from the degraded radiation pattern of the HAAwBE guarantees high success rates in the fault detection problem and high resolutions in the DoA estimation problem. Hence, our proposed techniques can significantly increase the speed of computations and calculations and reduce the cost of employing the complex radiation patterns in the existing technical literature [32], [33].

In this work, we have used the MATLAB programming platform to generate the raw data. Hence, we have imitated the raw data by sinusoidal functions, which are affected by the environmental noise, the coupling effect, and the wireless communication channel. In this work, the Ricean fading channel, line of sight (LoS), and equal correlation matrices have been assumed to model the real environment, as have been discussed in [34], for conditions of the wireless communication channel in this work.

A. FRAMEWORK OF THE RESEARCH PROBLEM

In this section, we aim to formulate the research problem under our proposed assumptions. Let us consider a superposition of electric fields resulting from all faulty and non-faulty elements of the HAAwBE in Eq. (2).

$$\mathbf{E} = \sum_{k=1}^{K} c_k \mathbf{E}_k = \sum_{k=1}^{K} \underbrace{a_k e^{-j\alpha_k}}_{c_k} \mathbf{E}_k, \quad \text{for} \quad k = 1, 2, \ldots, K \tag{2}$$

where a number of elements in the HAAwBE is assumed to be $K = 72$. Furthermore, each complex excitation of elements of c_k can be expanded in terms of its amplitude excitation of a_k and its phase excitation of α_k in Eq. (2). $\mathbf{E}_k$ denotes the complex electric field coefficient of kth element of the HAAwBE at the observation point.

Let us compute Eq. (3), given

- a degraded electric field resulting from the HAAwBE including only defective elements of $\Delta\mathbf{E}$,
- a measured electric field resulting from the HAAwBE including both faulty and radiating elements of $\mathbf{E}^H$, and
- an ideal electric field resulting from the HAAwBE including only radiating elements of $\mathbf{E}^I$,

$$\Delta\mathbf{E} = \mathbf{E}^H - \mathbf{E}^I = \sum_{k=1}^{K} \Delta a_k \mathbf{E}_k \tag{3}$$

where complex degraded excitations of elements of Δa_k in Eq. (3) can be expanded in terms of measured complex excitations of the HAAwBE and ideal complex excitations of the HAAwBE in Eq. (4).

$$\begin{aligned} \Delta c_k &= a_k^H e^{-j\alpha_k^H} - a_k^I e^{-j\alpha_k^I} \\ &= \left[a_k^H \cos\alpha_k^H - a_k^I \cos\alpha_k^I\right] - j\left[a_k^H \sin\alpha_k^H - a_k^I \sin\alpha_k^I\right] \end{aligned} \tag{4}$$

Let us consider the original signal of $\mathbf{x} \in \mathcal{S}^{2K+1}$ measured at outputs of 72 elements of the HAAwBE, in which $2K$ denotes the imaginary and real parts of element excitations. The measured signals at outputs of the HAAwBE also are affected by flaws and noise, and $\mathbf{x}$ shows a sparse approximation (or sparse representation) of signals of interest. K and L denote design parameters: the number of elements of the HAAwBE equal to 72 and the number of samples from the degraded radiation pattern equal to 25, respectively, where $L \ll K$.

Let us consider a linear operator of $\tilde{\mathbf{A}} \in \mathcal{C}^{2L\times 2K}$, and a set of measured radiation patterns of elements of the HAAwBE with a mathematical relationship of Eq. (5).

$$\tilde{\mathbf{R}} = \tilde{\mathbf{A}}\tilde{\mathbf{x}} + \tilde{\mathbf{e}} \tag{5}$$

The system of Eq. (5) includes the under-determined problem or an ill-posed inverse problem, in which coefficients of $\tilde{\mathbf{x}}$ are unknown, where $\tilde{\mathbf{R}} = \begin{bmatrix} Re(\mathbf{R}) \\ Im(\mathbf{R}) \end{bmatrix} \in \mathcal{S}^{2L\times 1}$, $\tilde{\mathbf{x}} = \begin{bmatrix} Re(\mathbf{x}) \\ Im(\mathbf{x}) \end{bmatrix} \in \mathcal{S}^{2K+1}$. It is assumed that there is a matrix of $\mathbf{w} \in \mathcal{C}^{2K\times 2K}$ orthogonal to $\mathbf{x}$ including multiple zero elements in terms of its dimensionality in the form of $\tilde{\mathbf{x}} := \mathbf{w}\mathbf{x}$.

$$\tilde{\mathbf{A}} = \begin{bmatrix} Re(\tilde{\mathbf{A}}) & -Im(\tilde{\mathbf{A}}) \\ Im(\tilde{\mathbf{A}}) & Re(\tilde{\mathbf{A}}) \end{bmatrix} \in \mathcal{C}^{2L\times 2K}$$

where the A_{lk} entry of $\tilde{A}$ denotes a product of the electric field factors of E_{lk} of the kth element at the lth measured sample.

$$\tilde{\mathbf{e}} = \begin{bmatrix} \mathbf{n} \\ \mathbf{e} \end{bmatrix} \in \mathcal{S}^{2L\times 1}$$

where $\mathbf{n}$ and $\mathbf{e}$ denote a $M \times 1$ matrix of noise and a $M \times 1$ matrix of zeros, respectively.

B. JOINT GROUP SPARSITY SETTING FOR THE ADMM TECHNIQUE

The discussion in the previous sub-section has focused on representing a framework of our problem. In this section, we aim to recover the signal of interest of $\tilde{\mathbf{x}}$ from a number of samples of the degraded electric field of $\tilde{\mathbf{R}}$ in the system of Eq. (5). Hence, to solve the regularized $l_{2,1}$-norm model of Eq. (1) for the system of Eq. (5), we have proposed the ADMM technique and decomposed it into its two convex quadratic primal and dual forms [32], [33].

To design the ADMM algorithm for Eq. (1), we outline the following preliminary information:

Preliminary 1: The signal ensembles are expressed in $2 \times K$ groups in Eq. (6).

$$x_{g_k} = \begin{bmatrix} x_{g_1} & x_{g_2} & \dots & x_{g_{2k}} \end{bmatrix} \in \mathcal{S}^{2K} \tag{6}$$

In the array signal processing framework, the ensemble of signals in Eq. (6) is expected to possess two types of joint structures: intra-signal correlation and inter-signal correlation. The intra-signal correlation is associated with the measured raw data at each HAAwBE element. In other words, components in each group of x_{g_k} are correlated and possess intra-signal correlation. In this work, in order to quantify and alleviate the effect of intra-signal correlation of measured signals at outputs of HAAwBE elements, we first produce sparse groups of projections onto a convex set. Then, a different model for Eq. (1) is trained within each of these groups using the Euclidean distance norm. The group-wise sparsity model is estimated by projections in the dual-based ADMM algorithm. We can also perform the *shrinkage* (i.e., compression along the normal axis of each measured datum) operation to produce the wise-group sparsity for variables in the primal-based ADMM algorithm.

Preliminary 2: The overlapping features in the x variable do not include difficulties in obtaining solutions. However, a further increase in the stability and reliability of solutions, we can consider Eq. (7).

$$\tilde{x} = Gx \tag{7}$$

where $G \in C^{2K \times 2K}$ possesses $0's$ and a single 1 in each of its rows.

Preliminary 3: The weighted $l_{2,1}$-regularization in Eq. (1) contains variables of ${x_{g_k}}'s$ with overlaps together, which provides more challenges to solve the problem. Hence, in order to employ the ADMM technique for the regularized $l_{2,1}$-norm problem, we first introduce an auxiliary variable of z in the group form of $z_k = x_{g_k}$ for $k = 1, 2, .., 2K$. Then, the ADMM algorithms are decomposed into quadratic convex sub-problems using the variable splitting technique in the form of $f_1(x) + f_2(z)$,

$$\begin{aligned} &\min_{x,z} f_1(x) + f_2(z) \\ &\text{s.t. } z = WGx \end{aligned} \tag{8}$$

where f_1 and f_2 are assumed to be quadratic and proximal functions. The deployment of the variable splitting technique transforms Eq. (1) to its equivalent problem in Eq. (9).

$$\begin{aligned} &\min \|\tilde{z}\|_{\omega,2,1} = \sum_{k=1}^{2K} \omega_k \|\tilde{z}_{g_k}\|_2 \\ &\text{s.t. } z_j = WGx_j, \tilde{\mathbf{A}}\tilde{\mathbf{x}} = \tilde{\mathbf{b}} \\ &\text{for } j = 1, 2, \dots, 2h \end{aligned} \tag{9}$$

Preliminary 4: Components in each group may include a wide dynamic range. We can significantly alleviate the effect of differences in scales of components by employing weights inside every group.

$$z_k = \mathbf{W}^{(2K)} x_{g_K} \quad k = 1, 2, \dots, 2K$$

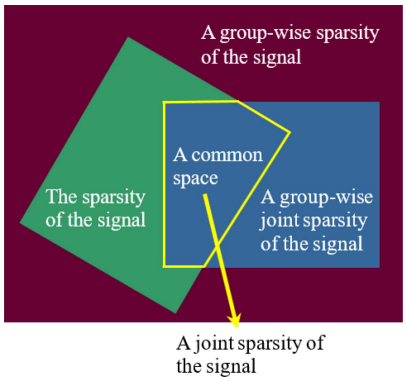

FIGURE 1. The Venn diagram for representing the relationship among a group-wise sparsity of the signal, a group-wise joint sparsity of the signal, a sparsity of the signal and a joint sparsity of the signal.

$$\mathbf{W}^{(2K)} \in C^{2K \times 2K} \tag{10}$$

where $\mathbf{z} = [z_1^T \; z_2^T \; \dots \; z_{(2K)}^T]^T \in \mathcal{S}^{2h}$ $G\mathbf{X}_{g_k} = [x_{g_1}^T \; x_{g_2}^T \; \dots \; x_{g_{(2K)}}^T]^T \in \mathcal{S}^{2h}$

$$\mathbf{W} := \begin{bmatrix} \mathbf{W}^{(1)} & & & \\ & \mathbf{W}^{(2)} & & \\ & & \ddots & \\ & & & \mathbf{W}^{(2K)} \end{bmatrix}$$

Therefore, results will show better stability and accuracy for both problems of fault detection and DoA estimation.

Preliminary 5: Structures of the overlapping group sparsity are caused by the presence of intra-signal correlation. Hence, to impose a further restriction on intra-signal correlation, and thereby generate non-overlapping group sparsity structures, a set of sparse solutions shares a common non-zero support in the same group. This model is called *joint sparsity*, as is illustrated in Figure 1.

Let us consider a collection h joint sparse solutions, such that each row of the solution matrix is devoted to a group.

Therefore, Eq. (9) is re-written for the joint sparsity structure of non-overlapping groups by the aforementioned modifications in Eqs. (11) to (14).

$$\begin{aligned} \tilde{\mathbf{A}} := \mathbf{I}_h \bigotimes \mathbf{A} = \begin{bmatrix} \mathbf{A}_1 & & & \\ & \mathbf{A}_2 & & \\ & & \ddots & \\ & & & \mathbf{A}_2 h \end{bmatrix}, \\ \mathbf{A}_j \in C^{l_j \times K} \quad (l_j < K) \end{aligned} \tag{11}$$

Standard notations of $\bigotimes$ and $vec(.)$ represent the Kronecker product and the vectorization of a matrix, respectively. The identity matrix of $\mathbf{I}_h \in C^{2h \times 2h}$ has been employed for transforming a vector of $\mathbf{A}$ to a matrix of $\tilde{\mathbf{A}}$.

$$\tilde{x} := vec(\mathbf{X}) = \begin{bmatrix} x_1 \\ x_2 \\ \vdots \\ x_{(2h)} \end{bmatrix} \tag{12}$$

$$\tilde{b} := vec(\mathbf{B}) = \begin{bmatrix} b_1 \\ b_2 \\ \vdots \\ b_{(2h)} \end{bmatrix} \tag{13}$$

where the observation vector $\tilde{b}$ is affect by noise. Indeed, the Basis Pursuit Denoising (BPD) technique of Eq. (9) has been implemented to decompose the collected signal at outputs of elements of the HAAwBE into its optimal superpositions.

1) A PRIMAL FORM OF THE ADMM TECHNIQUE BY THE JOINT SPARSITY SETTING

The ADMM technique by the joint sparsity setting has synthesized the augmented Lagrangian problem of Eq. (14) by minimizing the cost function of Eq. (9), with respect to variables of x and z, where $\Lambda_1 \in \mathcal{C}^{2K\times 1}$, $\Lambda_2 \in \mathcal{C}^{2L\times 1}$ denote multipliers and $\beta_1, \beta_2 > 0$ refer to penalty parameters.

$$\begin{aligned} \min_{x,z} \|z\|_{\omega,2,1} - \Lambda_1^T(z - WGx) + \frac{\beta_1}{2}\|z - WGx\|_2^2 \\ -\Lambda_2^T(\mathbf{A}x - b) + \frac{\beta_2}{2}\|\mathbf{A}x - b\|_2^2 \end{aligned} \tag{14}$$

To minimize the augmented Lagrangian problem of Eq. (14) with respect to variables of x and z alternating, we have decomposed the Lagrangian into the x-subproblem and z-subproblem.

x-subproblem: In Eqs. (15) to (17), we minimize the augmented Lagrangian problem of Eq. (14) with respect to the x variable.

$$\begin{aligned} \min_x \Lambda_1^T(\mathbf{Z} - WG\mathbf{X}) + \frac{\beta_1}{2}\|\mathbf{Z} - WG\mathbf{X}\|_2^2 \\ -\Lambda_2^T(\mathbf{A}\mathbf{X} - \mathbf{B}) + \frac{\beta_2}{2}\|\mathbf{A}\mathbf{X} - \mathbf{B}\|_2^2 \end{aligned} \tag{15}$$

$$\begin{aligned} \min_x \frac{1}{2}\mathbf{X}^T\Big[\beta_1(WG)(WG)^T\mathbf{I} + \beta_2\mathbf{A}\mathbf{A}^T\Big]\mathbf{X} \\ = \Big(-\Lambda_1 + \beta_1(WG)\mathbf{Z}\mathbf{A}\mathbf{A}^T\Big)^T\mathbf{X} \end{aligned} \tag{16}$$

$$\begin{aligned} \mathbf{X} = \Big[\beta_1(WG)(WG)^T\mathbf{I} + \beta_2\mathbf{A}^T\mathbf{A}\Big]^{-1} \\ \Big[-\Lambda_1(WG)^T + \beta_1(WG)^T\mathbf{Z} + \Lambda_2\mathbf{A}^T + \beta_2\mathbf{A}^T\mathbf{B}\Big] \end{aligned} \tag{17}$$

z-subproblem:

$$\min_Z \|\mathbf{Z}\|_{\omega,2,1} - \Lambda_1^T\mathbf{Z} + \frac{\beta_1}{2}\|\mathbf{Z} - WG\mathbf{X}\|_2^2 \tag{18}$$

$$\min_Z \|\mathbf{Z}\|_{\omega,2,1} - \Lambda_1^T\mathbf{Z} + \frac{\beta_1}{2}(\mathbf{Z} - WG\mathbf{X})^T(\mathbf{Z} - WG\mathbf{X}) \tag{19}$$

The closed-form solution to minimize the z-subproblem consists of the row-wise shrinkage in one dimension in Eqs. (19) and (20).

$$z^k = \max\left\{\left\|r^k\right\|_2 - \frac{\omega_k}{\beta_1}, 0\right\}\frac{r^k}{\left\|r^k\right\|_2}, \quad \text{for} \quad k = 1, 2, \ldots, 2K \tag{20}$$

Algorithm 1: Primal-Based ADMM Scheme for the Joint Sparsity Setting

1) Initialize:
   $Z \in \mathcal{C}^{2K}$, $\Lambda_1 \in \mathcal{C}^{2K\times 1}$, $\Lambda_2 \in \mathcal{C}^{2L\times 1}$, $\beta_1, \beta_2 > 0$, $\gamma_1, \gamma_2 > 0$
   Updating variables and parameters
2) $\mathbf{X} \leftarrow [\beta_1(WG)(WG)^T\mathbf{I} + \beta_2\mathbf{A}^T\mathbf{A}]^{-1}[-\Lambda_1(WG)^T + \beta_1(WG)^T\mathbf{Z} + \Lambda_2\mathbf{A}^T + \beta_2\mathbf{A}^T\mathbf{B}]$
3) $\mathbf{Z} \leftarrow shrink(\mathbf{X} + \frac{\Lambda_1}{WG\beta_1}, \frac{1}{\beta_1}\mathbf{W})$
4) $\Lambda_1 \leftarrow \Lambda_1 - \gamma_1\beta_1(\mathbf{Z} - WG\mathbf{X})$
5) $\Lambda_2 \leftarrow \Lambda_2 - \gamma_2\beta_2(\mathbf{A}\mathbf{X} - \mathbf{B})$

where x^k and ω_k represent the ith row of the matrix of $\mathbf{X}$ and kth column of the matrix of W, respectively.

$$r^k := (WG)x^k + \frac{\lambda_1^k}{\beta_1} \tag{21}$$

Consequently, we have minimized the cost function of Eq. (14) in both directions of z and x simultaneously at each iteration, as outlined in 1.

2) A DUAL FORM OF THE ADMM TECHNIQUE BY THE JOINT SPARSITY SETTING

Here, the ADMM technique by the joint sparsity setting has built the augmented Lagrangian problem in Eq. (23) by minimizing the cost function of Eq. (9).

$$\begin{aligned} &\min_{y,z} -b^T y \\ &\text{s.t. } z = \mathbf{A}^T y, \\ &\qquad \|z_{g_k}\|_2 \le w_i \quad \text{for} \quad k = 1, 2, \ldots, 2K \end{aligned} \tag{22}$$

$$\begin{aligned} &\min_{y,z} -b^T y - x^T\Big(z - WG\mathbf{A}^T y\Big) + \frac{\beta}{2}\Big\|z - WG\mathbf{A}^T y\Big\|_2^2 \\ &\text{s.t.} \quad \|z_{g_k}\|_2 \le w_k \quad \text{for} \quad k = 1, 2, \ldots, 2K \end{aligned} \tag{23}$$

z-subproblem: The group-wise projections on a convex set have been estimated to solve the z-subproblem of the ADMM dual algorithm in Eqs. from (25) to (26).

$$-\mathbf{B}^T\mathbf{Y} - \mathbf{X}^T\Big(\mathbf{Z} - WG\mathbf{A}^T\mathbf{Y}\Big) + \frac{\beta}{2}\Big\|\mathbf{Z} - WG\mathbf{A}^T\mathbf{Y}\Big\|_2^2 \tag{24}$$

$$z_{g_k} = \rho_{p_2^i}\left(\frac{1}{\beta}x_{g_k} + WG\mathbf{A}_{g_k}^T y\right) \quad \text{for} \quad k = 1, 2, \ldots, K \tag{25}$$

$$\rho_{p_2^i} \triangleq \Big\{z \in \mathcal{S}^{2K} : \|z\|_2 \le w_k\Big\} \tag{26}$$

where $\beta > 0$.

y-subproblem: To reduce the computation time, the proposed solutions for the y-subproblem are limited to the following two scenarios:

- when A is characterized by an orthonormal matrix: The gradient descent steps were taken in terms of the y variable, as a variable of the dual problem, towards a vector space in which constraints of the dual problem hold.

Algorithm 2: Dual-Based ADMM Scheme for the Joint Sparsity Setting

1) Initialize:
   $\mathbf{X} \in \mathcal{S}^{2K}, \mathbf{Z} \in \mathcal{S}^{2K}, \beta > 0, \gamma > 0$
   Updating variables and parameters
2) $\mathbf{Y} \leftarrow [\beta(\mathbf{A}\mathbf{A}^T)(WG)(WG)^T]^{-1}[\mathbf{B} - (WG)\mathbf{A}\mathbf{X} + \beta\mathbf{A}(WG)^T\mathbf{Z}]$
3) $\mathbf{Z} \leftarrow \rho_{p_2}\left((WG)\mathbf{A}^T\mathbf{Y} + \frac{1}{\beta}\mathbf{X}\right)$
4) $\mathbf{\Lambda_1} \leftarrow \mathbf{\Lambda_1} - \gamma_1\beta_1(\mathbf{Z} - WG\mathbf{X})$
5) $\mathbf{\Lambda_2} \leftarrow \mathbf{\Lambda_2} - \gamma_2\beta_2(\mathbf{A}\mathbf{X} - \mathbf{B})$

- when A is characterized by a non-orthonormal matrix: we have employed exact computations including the $A.inVAAT$ operator and the $YALL1-Group$ solver, as represented in Algorithm 2.

$$\begin{aligned}&\max_y\left\{\min_x \sum_{k=1}^{K}\|x_{g_k}\|_2 - y^T(\mathbf{A}x - b)\right\}\\ &= \max_y\left\{b_y^T + \min_x \sum_{k=1}^{K}\left(w_k\|x_{g_k}\|_2 - y^T\mathbf{A}_{g_k}x_{g_i}\right)\right\}\\ &= \max_y\left\{b_y^T : \left\|\mathbf{A}_{g_k}^T y\right\|_2 \le w_k, \quad \text{for} \quad k = 1, 2, \ldots, 2K\right.\end{aligned} \tag{27}$$

where $y \in \mathcal{S}^{2L}$, and $\mathbf{A}_{g_k}^T$ denotes a sub-matrix, which is composed of columns of $\mathbf{A}$ and associated with the kth group.

$$\min_y -b^T y + WG(\mathbf{A}x)^T y + \frac{\beta}{2}\left\|z - (WG)\mathbf{A}^T y\right\|_2^2 \tag{28}$$

$$\beta\left(\mathbf{A}\mathbf{A}^T\right)(WG)(WG)^T\mathbf{Y} = \mathbf{B} - (WG)\mathbf{A}\mathbf{X} + \beta\mathbf{A}(WG)^T\mathbf{Z} \tag{29}$$

Consequently, the ADMM algorithm can reconstruct the joint sparse signal in the presence of defective elements of the HAAwBE with high probability and accuracy by solving Eq. (1) when step sizes satisfy the upper bound for a theoretical convergence criterion, which is equal to 1.618.

C. OPTIMIZATION MODELS

The discussion in the previous sub-section has focused on providing quadratic convex solutions for Eq. (1). In the following, we aim to train the three different models, LS-SVM, NN-RBF, and NN-MLP, by the parameters, hyper-parameters, and variables of the proposed ADMM technique to overcome the limitations of their existing training algorithms. The trained parameters of the ADMM algorithm are configured for the neural networks and LS-SVM model in the form of weight matrices along with activation functions. Activation functions would be expected to represent the non-linearity of the problem, however the optimal parameters are linear. Each group of neurons include similar inputs, however, different weights. Each layer is constructed by a group of neurons.

It is worth mentioning that the initialization performance and stability of three of the optimization techniques, discussed in this sub-section, degrade because the iterative shrinkage provides additional training variables for them. However, the initialization strategies and update approaches of all three proposed optimization methods are able to manage the minimization of the z-subproblems of the ADMM technique within the training process. Hence, in this work, updating hyper-parameters associated with the shrinkage operation and step sizes are performed by the three optimization models within their training procedures.

The presence of extreme data sparseness in the given dataset collected from 72 outputs of elements of the HAAwBE results from errors in element excitations. The excitation phases and amplitudes of elements of the HAAwBE have sparse representations, whose few non-zero coefficients can be divided in groups. This section has focused on performing the joint group sparse reconstruction of high dimensional data from a limited sample set of HAAwBE degraded radiation patterns.

The main task of the proposed pattern recognition algorithms for both problems of fault detection and DoA estimation consists of assigning class labels to measurement vectors or feature extraction. For instance, in a general classification algorithm, a set of features is extracted from a few samples of the degraded radiation pattern of the HAAwBE, which is capable of being classified and relevant to the involved problem. Generally, the set of features for each given HAAwBE radiation pattern is expressed by vectors.

The three general steps for the fault detection problem for all three models of LS-SVM, NN-RBF, and NN-MLP include:

Labeling data: Labeling is performed by the data from the ideal hybrid antenna array (or the hybrid antenna array without any faulty elements) that is characterized by the mask field (MF) in Figures 3.

Classifying data: The optimization methods have been performed for classifying the data from HAAwBE element outputs. In this sense, each class is allocated for each individual array element.

Finding defective array elements: When an error between the labeled data and classified data is more than one threshold, the classified data is associated with a faulty array element.

We have illustrated the 3D configuration of the HAAwBE in Figure 2. As described in detail in [9], [10], the radiation characteristics of the HAAwBE consist of several different advantages including high directivity and gain, deep nulls, the superior performance and high resolution for the DoA estimation problem, and uniform 3D spherical coverage, which make it a potential candidate for beamforming, beamsteering, and nullsteering applications.

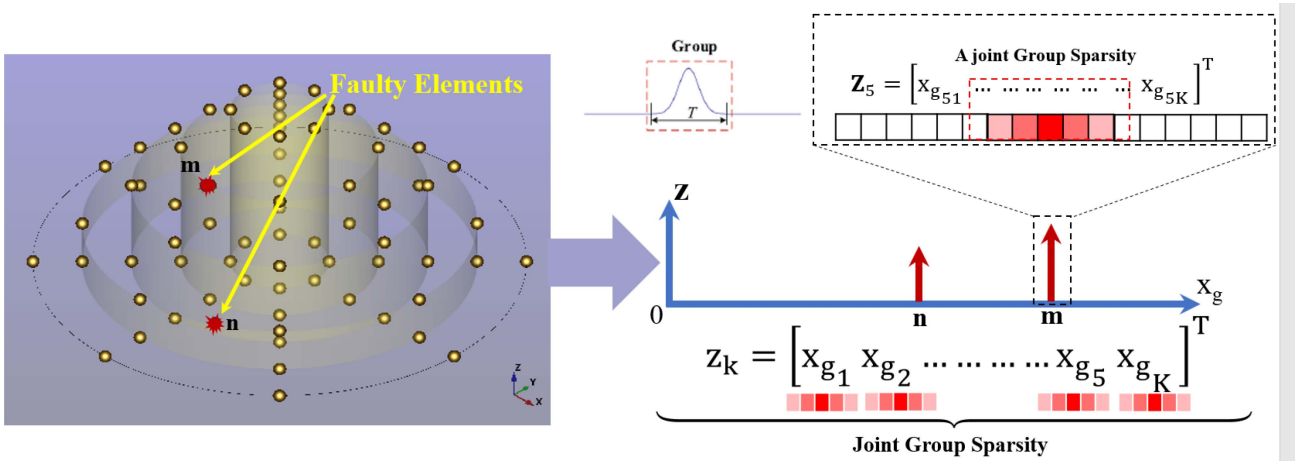

FIGURE 2. A 3D view of the HAAwBE at an operating frequency of 10 GHz. It consists of one circular antenna array in the xy-plane and one cylindrical antenna array along with the z-axis [35]. We also have represented the joint group sparsity in the presence of two faulty elements in the HAAwBE.

1) FAULT DETECTION AND DOA ESTIMATION: NEURAL NETWORKS

Although architectures of MLP neural networks appear to be similar to RBF neural networks, there are significant differences between their functionalities. For instance, a distinct difference, which is noticeable between the two networks of NN-RBF and NN-MLP, results from their feeding inputs. Measurements of distances between inputs and the hidden layer are transferred through the RBF optimization method rather than raw data. In other words, RBF models employ Euclidean distances for processing data, however, MLP models compute inner products, which can be computationally intensive. Here, we have represented a similar technique for training models of NN-RBF and NN-MLP, rather than their conventional training techniques, in Eq. (30).

$$\begin{aligned} \mathcal{X}_1 &= h_1(z_1) \\ \mathcal{X}_2 &= h_2(z_2) \\ &\vdots \\ \mathcal{X}_5 &= h_5(z_5) \end{aligned} \tag{30}$$

the activation function h_l in each of the five hidden layers is activated by the variables x and z of the primal form of the ADMM technique. Moreover, the step size, regularization parameter, and quadratic penalty parameters are effectively updated to minimize errors between the mask function of $MF(\Theta_m, \Phi_n)$ and $FF(\Theta_m, \Phi_n)$s, 3.

2) FAULT DETECTION AND DOA ESTIMATION: LS-SVM MODEL

Here, we aim to describe how the LS-SVM algorithm can be trained with the ADMM technique. Although the training procedure of the LS-SVM model is performed on a convex optimization problem, the computation of kernel matrices degrade the LS-SVM performance, especially for large-scale and non-linear problems. Hence, as represented in

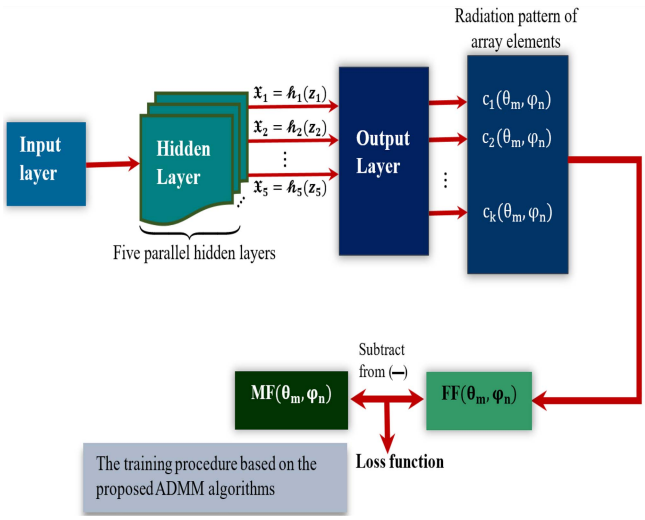

FIGURE 3. A general architecture to illustrate the training procedure of models of the NN-MLP and NN-RBF based on the proposed ADMM technique. Here, we did not consider the differences between the interior architectures of NN-MLP and NN-RBF models. The mask function of $MF(\Theta_m, \Phi_n)$ denotes an ideal radiation pattern of the HAAwBE without any defective elements. The far-field function of $FF(\Theta_m, \Phi_n)$ represents a sample of the degraded radiation pattern which trained by either the NN-MLP or NN-RBF.

Eq. (31), the LS-SVM model can be effectively trained by the estimated parameters, hyper-parameters, and variables of the ADMM technique.

$$(\mathbf{y}_{\text{test}})_j = \text{sign}\left[\sum_{k=1}^{K} (\mathbf{z})_k \mathbb{K}\big((x_{\text{train}})_k, (x_{\text{test}})_j\big) + b\right], \quad \text{for} \quad j = 1, 2, \dots, J \tag{31}$$

where $\mathbb{K}$ and $\mathbf{J}$ denote the kernel function, and a number of data points in the testing dataset. The relationship between the trained model of Y_{train}, which is obtained by the dual form of the ADMM technique, and the variable z, which results from the primal form of the ADMM technique, is

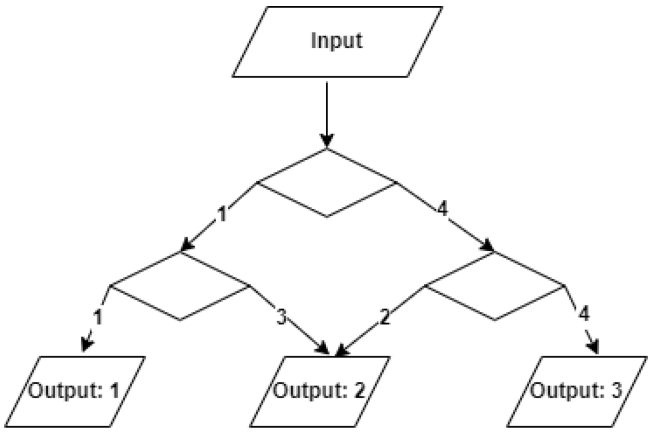

FIGURE 4. The architecture of the three-class DDAG technique, which employs the one-vs-one multi-class classification algorithm, for the DoA estimation, as described in detail in [8].

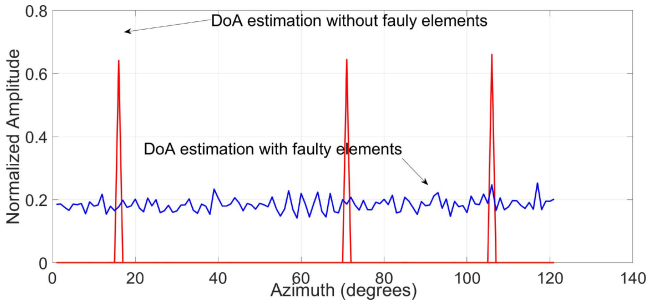

FIGURE 5. Results of DoA estimation with performing the LS-SVM for the HAAwBE, consistent with Figure 2, at an operating frequency of 10 GHz. It is assumed that there are 12 radiating elements, and 60 non-radiating (defective) elements, which is accompanied by the presence of 83% faulty elements. Also, we took 25 samples from the degraded radiation pattern of the HAAwBE with 72 elements.

expressed in Eq. (32)

$$\mathbf{Z}_y = Y_{\text{train}}\mathbf{Z}^{\text{MaxIt}} \tag{32}$$

z^{MaxIt} represents a value z in which both variables z and x were minimized in the primal form of the ADMM technique. Moreover, the estimated parameter *MaxIt* by the ADMM technique allows for enhancing the classification accuracy and immutability of the proposed approach in both problems of DoA estimation and fault detection, as discussed in the next section.

IV. NUMERICAL RESULTS AND DISCUSSION

In this section, we have deployed the three models of NN-MLP, NN-RBF, and LS-SVM, which we trained by the ADMM technique, to problems of DoA estimation and fault detection. The proposed methodology has been described in the previous section. In response to the question of which features of an antenna array can be useful for discriminating radiating elements from no-radiating elements, we have chosen 25 samples of the degraded radiation pattern of the HAAwBE. Then, we have verified that the deployment of the three models for the 3D configuration of the HAAwBE, not only provides significant discrimination between the amplitudes of faulty and radiating elements, but also identifies locations of faulty elements. Hence, this section addresses how deploying the optimization models enhances the HAAwBE performance in problems of DoA estimation and fault detection. Then, by estimating success rates for the three models, we have analogously evaluated their performance in recognizing locations of sources.

A. DOA ESTIMATION AND FAULT DETECTION

Any modifications and changes in the total far-field radiation pattern of the HAAwBE can be equivalently extended to all other far-field problems such as DoA estimation and fault detection. Without performing any optimization method, the HAAwBE is not capable of recognizing locations of sources in the presence of 83% faulty elements. As Figure 5 illustrates, the blue plot of DoA estimation includes periodic variations around its normalized expected mean value of 0.25. However, the HAAwBE with the LS-SVM model has recognized the locations of three sources at 16°, 71°, and 106°, with the normalized amplitudes of 0.642, 0.664, 0.660, respectively, with a very high resolution.

B. EFFECTS OF FAULTY ELEMENTS ON THE ANTENNA ARRAY PERFORMANCE

In this study, fault detection has been fulfilled based on exploring the far-field radiation pattern and taking 25 samples of the degraded radiation pattern of the HAAwBE in the presence of faulty elements. Simulation results in Figure 6 show that amplitudes of the received energy reduce in the faulty elements, however, the estimator tool is not capable of discriminating between amplitudes of non-radiating and radiating elements. It is evident how received energies are significantly degraded in the HAAwBE by the presence of 50% faulty elements in Figure 6 (a). A major difference in the accuracy and robustness of the performance of fault detection in the HAAwBE, resulting from higher received energies, is noticeable by deploying the LS-SVM technique, Figure 6 (c), compared to the NN-RBF technique, Figure 6 (b).

Amplitudes have shown in Figures 7 to 9, and Tables 2 to 4 improved performance of the HAAwBE by performing the NN-RBF model in the presence of faulty elements, compared to the two other models. Here, it is even more evident how the HAAwBE performance with the NN-RBF model degrades when subjected to a higher number of faulty elements, and is enhanced in the presence of fewer faulty elements.

Figure 8 and Table 3 reports that the NN-MLP model could enhance the HAAwBE performance for the fault detection problem in the presence of faulty elements. It is evident how deploying the NN-MLP model, despite an increase in the number of faulty array elements, enhances the SLLs and makes nulls deeper. Hence, the NN-MLP model becomes even more efficient when the numbers of faulty elements increase.

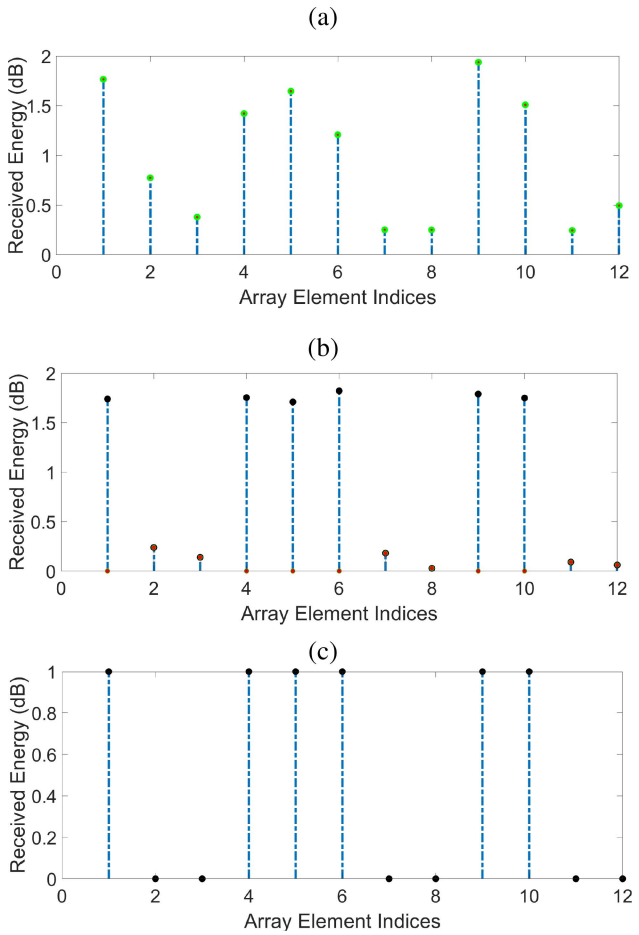

FIGURE 6. Variations of received energies for all radiating and non-radiating elements of the HAAwBE, consistent with Figure 2, in the presence of 50% faulty elements at an operating frequency of 10 GHz: (a) without performing any optimization methods, (b) with performing the RBF technique, and (c) with performing the LS-SVM technique. The total number of elements of the HAAwBE is supposed to be 12. Furthermore, faulty elements are located at positions 2, 3, 7, 8, 11, and 12. Higher received energies imply better accuracy and robustness of the HAAwBE in fault detection.

TABLE 2. Variations in the HAAwBE performance by implementing the RBF model in the presence of the three different numbers of faulty elements of 1 (as a low number), 5 (as a medium number), and 10 (as a high number) at an operating frequency of 10 GHz and $\phi = 0°$. Here, the total number of array elements of the HAAwBE, consistent with Figure 2, is assumed to be 30.

		1 faulty element (Low)	5 faulty elements (Medium)	10 faulty elements (High)
Normalized amplitude	Mainlobe	1.000 at $-67°$	1.000 at $-43°$	0.917 at $68°$
	Sidelobe	0.164 at $-80°$	0.237 at $-56°$	0.189 at $79°$
	SLL	0.836	0.763	0.728
	First null	0.028 at $-60°$	0.038 at $-52°$	0.041 at $61°$
Phase angle (degree)	ON	$180°$	$60°$	$144°$
	OFF	$-174°$	$-120°$	$-36°$
	|ON-OFF|	$354°$	$180°$	$180°$

TABLE 3. Variations in the HAAwBE performance by implementing the NN-MLP model in the presence of the three different numbers of faulty elements of 1 (as a low number), 5 (as a medium number), and 10 (as a high number) at an operating frequency of 10 GHz and $\phi = 0°$. Here, the total number of array elements of the HAAwBE, consistent with Figure 2, is assumed to be 30.

		1 faulty element (Low)	5 faulty elements (Medium)	10 faulty elements (High)
Normalized amplitude	Mainlobe	1.0000 at $45°$	1.0000 at $-55°$	1.0000 at $-68°$
	Sidelobe	0.5229 at $22°$	0.6135 at $-45°$	0.1957 at $-56°$
	SLL	0.5229	0.3865	0.8043
	First null	0.0268 at $63°$	0.5754 at $-48°$	0.0197 at $-61°$
Phase angle (degree)	ON	$180°$	$90°$	$150°$
	OFF	$-180°$	$-99°$	$-47°$
	|ON-OFF|	$360°$	$189°$	$197°$

Figure 9 and Table 4 ensure that the HAAwBE performance with deploying the LS-SVM model is enhanced when the number of faulty elements remains medium. In other words, the HAAwBE performance, with the LS-SVM model in terms of enhancing SLLs and making deeper nulls, is substantially improved when the number of faulty elements is equal to five (or a medium number of faulty elements), compared to the presence of low and high numbers of faulty elements.

Furthermore, it is noticeable in Figures 7 to 9, where the number of faulty elements change, locations of mainbeams shift.

Consequently, we can conclude that the HAAwBE effectiveness and performance by performing each optimization model vary with respect to changes in the number of faulty array elements. An increase in the number of non-radiating elements, despite the HAAwBE and its radiation pattern deterioration, is accompanied by a reduction in computational complexity and data processing from the lower number of radiating elements in its involved optimization method. In other words, a higher number of radiating elements may cause more non-linearity and higher complexities of the data processing procedure in its involved optimization method.

Hence, since the NN-MLP model is more compatible for the linearly-separable data, the HAAwBE with the NN-MLP model shows better performance in the presence of higher numbers of faulty elements. However, hidden layers in the RBF model can perform non-linear data processing and thereby show better performance for the HAAwBE in the higher numbers of radiating elements.

C. SUCCESS RATE

A metric of success rate denotes how well an antenna array can discriminate non-radiating elements from radiating elements and recognize locations of faulty elements. A higher success rate implies that the antenna array possesses higher

TABLE 4. Variations in the HAAwBE performance by implementing the LS-SVM model in the presence of the three different numbers of faulty elements of 1 (as a low number), 5 (as a medium number), and 10 (as a high number) at an operating frequency of 10 GHz and $\phi = 0°$. Here, the total number of array elements of the HAAwBE, consistent with Figure 2, is assumed to be 30.

		1 faulty element (Low)	5 faulty elements (Medium)	10 faulty elements (High)
Normalized amplitude	Mainlobe	1.0000 at $-12°$	1.0000 at $59°$	0.9984 at $-46°$
	Sidelobe	0.5826 at $-23°$	0.2461 at $68°$	0.7350 at $-23°$
	SLL	0.4174	0.7539	0.2634
	First null	0.0117 at $-6°$	0.1035 at $65°$	0.0579 at $-37°$
Phase angle (degree)	ON	$180°$	$6°$	$144°$
	OFF	$-174°$	$-174°$	$-36°$
	|ON-OFF|	$354°$	$180°$	$180°$

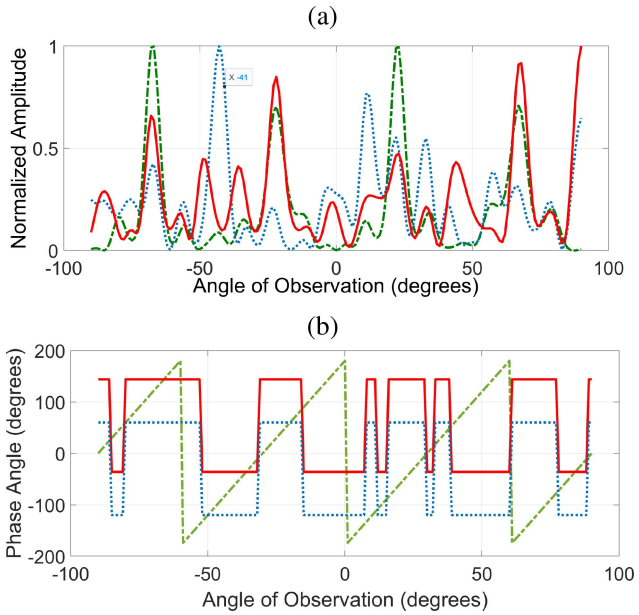

FIGURE 7. We have implemented the RBF technique for determining locations, including phases and amplitudes, of array elements in the HAAwBE, consistent with Figure 2, with the presence of one faulty element, five faulty elements, and ten faulty elements at an operating frequency of 10 GHz and $\phi = 0°$. Green, blue, and red graphs are respectively associated with the presence of 1, 5, and 10 faulty elements in the HAAwBE: (a) variations of normalized amplitudes of the HAAwBE radiation patterns in terms of angles of observation, and (b) variations of phase angles of array elements in terms of angles of observation. Maximum phases denote locations of radiating elements or "ON" states while minimum phases refer to non-radiating elements or "OFF" states. It is assumed that the total number of array elements of the HAAwBE is equal to 30.

resolution and more invariance in the presence of faulty elements, [36]. An optimization model in any antenna array with a lower success rate may fail to provide a solution with high precision. Hence, we have further verified the immutability and accuracy of the HAAwBE performance with performing the three optimization models of NN-RBF, NN-MLP, and LS-SVM in the fault detection problem using the metric of the success rate of 91.83%, 91.24%, and

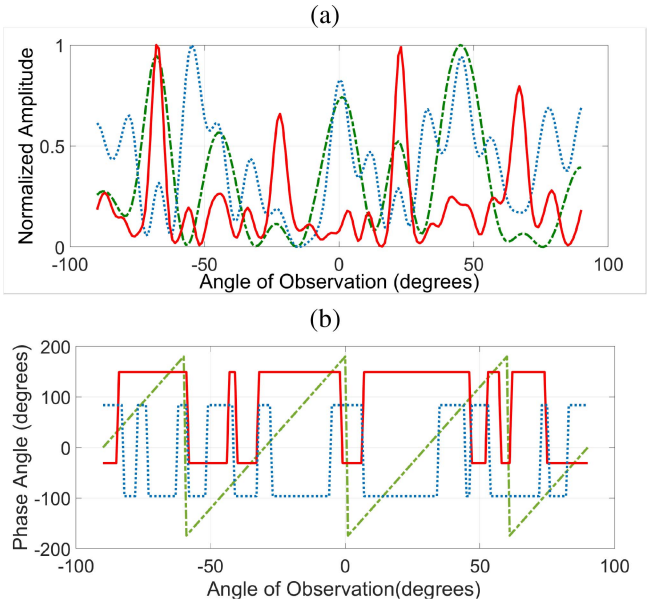

FIGURE 8. We have implemented the MLP model for determining locations, including phases and amplitudes, of array elements in the HAAwBE, consistent with Figure 2, in the presence of one faulty element, five faulty elements, and ten faulty elements at an operating frequency of 10 GHz and $\phi = 0°$. Green, blue, and red graphs are respectively associated with the presence of 1, 5, and 10 faulty elements in the HAAwBE: (a) variations of normalized amplitudes of the HAAwBE radiation patterns in terms of angles of observation, and (b) variations of phase angles of array elements in terms of angles of observation. Maximum phases denote locations of radiating elements or "ON" states while minimum phases refer to non-radiating elements or "OFF" states. It is assumed that the total number of array elements of the HAAwBE is equal to 30.

88.23%, respectively, in the presence of 50% faulty elements, as reported in Figure 10.

Figure 10 has reported that the deployment of all three optimization models for the HAAwBE possesses high success rates for the fault detection problem. These high values of the success rates can guarantee that the HAAwBE is capable of recognizing locations of radiating elements from non-radiating elements with high resolution.

V. CONCLUSION

To conclude, in this research study, some of the current techniques and solutions for fault detection and DoA estimation have been outlined and reviewed. We have deployed the three different LS-SVM, NN-MLP, and NN-RBF, for the HAAwBE to solve the regularized $l_{2,1,w}$-norm problem for fault detection and DoA estimation. However, conventional neural networks and LS-SVM models have relied on gradient-based computation and back-propagation. Hence, these conventional models possess sequential dependencies and thereby are not appropriate for hardware accelerations. Since we have trained the NN-MLP, NN-RBF, and LS-SVM models with the ADMM method, they do not rely on gradient-based computation and the back-propagation, and therefore can be effectively parallelized. This renders our approach more suitable for hardware implementation.

Moreover, the effectiveness of the three different optimization models varies in terms of the percentage of

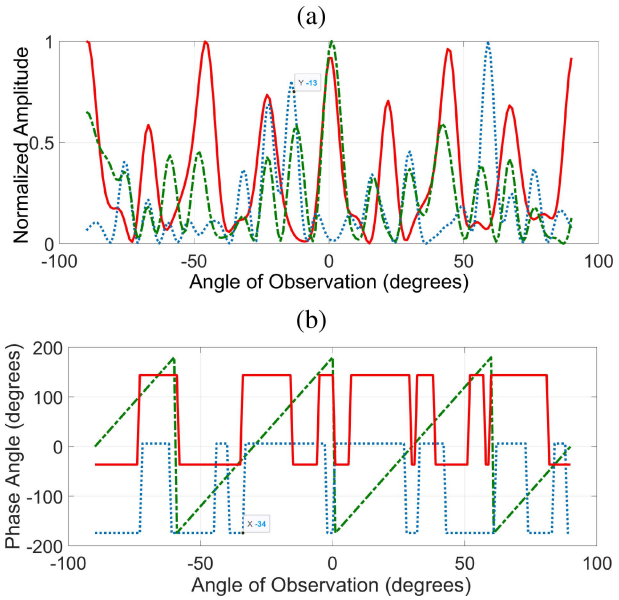

FIGURE 9. We have implemented the LS-SVM model for determining locations, including phases and amplitudes, of elements in the HAAwBE in the presence of one faulty element, five faulty elements, and ten faulty elements at an operating frequency of 10 GHz and $\phi = 0°$. Green, blue, and red graphs are respectively associated with the presence of 1, 5, and 10 faulty elements in the HAAwBE: (a) variations of normalized amplitudes of the HAAwBE radiation patterns in terms of angles of observation, and (b) variations of phase angles of array elements in terms of angles of observation. Maximum phases denote locations of radiating elements or "ON" states while minimum phases refer to non-radiating elements or "OFF" states. It is assumed that the total number of array elements of the HAAwBE is equal to 30.

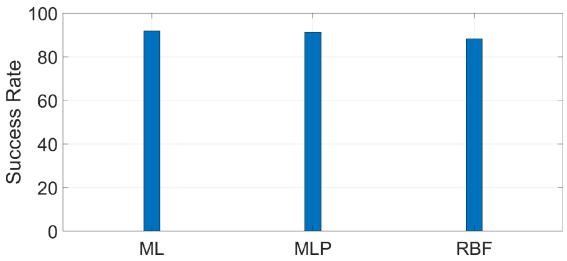

FIGURE 10. Variations of the success rates of the three different optimization models of NN-RBF, NN-MLP, and three-class classification LS-SVM. In this sense, the optimization models have been implemented for the HAAwBE of Figure 2 in the presence of about 50% faulty elements. The total number of the HAAwBE is supposed to be 12.

non-radiating array elements in the HAAwBE. Numerical results have confirmed that the NN-RBF, LS-SVM, and NN-MLP models yield better performance in the presence of low, medium, and high percentages of non-radiating array elements, respectively.

We have verified that it is practically infeasible to achieve DoA estimation without performing any optimization methods in the presence of a high number of non-radiating elements. However, the implementation of the three-class classification LS-SVM technique for the HAAwBE could significantly enhance the performance of the DoA estimation with high resolution.

We also presented that, in practical scenarios, as the percentage of faulty elements increases, the feasibility recognizing faulty elements from non-faulty elements becomes more challenging. However, performing the three-class classification LS-SVM model for the 3D HAAwBE could effectively determine the locations of faulty elements.

In addition, the success rates of these three optimization models in the presence of about 50% faulty elements (or medium) have verified the much more invariance and accuracy in the LS-SVM model compared to the two other neural network models.

In the framework of the array signal processing, we believe that the concept of fault detection may become of major interest for all antenna arrays. The recent progress in optimization methods may soon open up possibilities for enhancing the performance of antenna arrays in the presence of a high percentage of faulty elements.

ACKNOWLEDGMENT

The authors wish to express our appreciation to the ONR for its generous support of this research project.

REFERENCES

[1] A. J. van den Biggelaar, U. Johannsen, P. Mattheijssen, and A. B. Smolders, "Improved statistical model on the effect of random errors in the phase and amplitude of element excitations on the array radiation pattern," *IEEE Trans. Antennas Propag.*, vol. 66, no. 5, pp. 2309–2317, May 2018.

[2] H. P. J. A. Rodríguez, F. Ares, and J. Vassal'lo, "Finding defective elements in planar arrays using genetic algorithms—Abstract," *J. Electromagn. Waves Appl.*, vol. 14, no. 6, pp. 827–828, 2000.

[3] O. Bucci, A. Capozzoli, and G. D'Elia, "Diagnosis of array faults from far-field amplitude-only data," *IEEE Trans. Antennas Propag.*, vol. 48, no. 5, pp. 647–652, May 2000.

[4] A. Wuraola and N. D. Patel, "Computationally efficient radial basis function," in *Proc. Int. Conf. Neural Inf. Process.*, 2018, pp. 103–112.

[5] F. Amato, N. Mazzocca, F. Moscato, and E. Vivenzio, "Multilayer perceptron: An intelligent model for classification and intrusion detection," in *Proc. 31st Int. Conf. Adv. Inf. Netw. Appl. Workshops (WAINA)*, 2017, pp. 686–691.

[6] J. Rohwer and C. Abdallah, "Support vector machines for direction of arrival estimatio," 2012, Pre print. [Online]. Available: https://digitalrepository.unm.edu/ece_fsp/36

[7] J. Ronen and R. Clarke, "Monitoring techniques for phased-array antennas," *IEEE Trans. Antennas Propag.*, vol. 33, no. 12, pp. 1313–1327, Dec. 1985.

[8] C. T. Abdallah, "Defense technical information center compilation part notice ADP 014209 title: One-vs-one multiclass least squares support vector machines for direction of arrival estimation," *Appl. Comput. Electromagn. Soc. J.*, vol. 18, no. 2, pp. 1054–4887, 2003.

[9] X. Zhang et al., "Integrated broadband bowtie antenna on transparent silica substrate," *IEEE Antennas Wireless Propag. Lett.*, vol. 15, pp. 1377–1381, 2016.

[10] R. Sahoo and D. Vakula, "Bow-tie-shaped wideband conformal antenna with wide-slot for GPS application," *Turkish J. Electr. Eng. Comput. Sci.*, vol. 27, no. 1, pp. 80–93, 2019.

[11] M. Haurthi and B. Rao, "All-pole modeling of speech based on the minimum variance distortionless response spectrum," in *Proc. Conf. Record 31st Asilomar Conf. Signals, Syst. Comput.*, vol. 2, 1997, pp. 1061–1065.

[12] V. Behar, C. Kabakchiev, and H. Rohling, "MVDR radar signal processing approach for jamming suppression in satellite navigation receivers," in *Proc. 11th Int. Radar Symp.*, 2010, pp. 1–4.

[13] K. Worden and J. Dulieu-Barton, "An overview of intelligent fault detection in systems and structures," *Struct. Health Monit.*, vol. 3, no. 1, pp. 85–98, 2004.

[14] R. Isermann, "Model-based fault-detection and diagnosis—Status and applications," *Annu. Rev. Control*, vol. 29, no. 1, pp. 71–85, 2005.

[15] C. Persis and A. Isidori, "A geometric approach to nonlinear fault detection and isolation," *IEEE Trans. Autom. Control*, vol. 46, no. 6, pp. 853–865, Jun. 2001.

[16] W. Deng, W. Yin, and Y. Zhang, "Group sparse optimization by alternating direction method," in *Proc. 15th SPIE Wavel. Sparsity*, 2013, pp. 242–256.
[17] Y. Xiao, H. Zhu, and S.-Y. Wu, "Primal and dual alternating direction algorithms for l1-l1-norm minimization problems in compressive sensing," *Comput. Optim. Appl.*, vol. 54, pp. 441–459, Mar. 2013.
[18] J. A. Rodriguez-Gonzalez, F. Ares-Pena, M. Fernandez-Delgado, R. Iglesias, and S. Barro, "Rapid method for finding faulty elements in antenna arrays using far field pattern samples," in *Proc. 3rd Eur. Conf. Antennas Propag.*, 2009, pp. 3380–3384.
[19] K. Muzaffar, L. I. Giri, K. Chatterjee, S. Tuli, and S. Koul, "Fault detection of antenna arrays using infrared thermography," *Infrared Phys. Technol.*, vol. 71, pp. 464–468, Jul. 2015. [Online]. Available: https://www.sciencedirect.com/science/article/pii/S1350449515001474
[20] N. Boopalan, A. K. Ramasamy, and F. Nagi, "A comparison of faulty antenna detection methodologies in planar array," *Appl. Sci.*, vol. 13, no. 6, p. 3695, 2023. [Online]. Available: https://www.mdpi.com/2076-3417/13/6/3695
[21] D. J. van Rensburg, *Limitations of Near-Field Back Projection for Phased Array Tuning Applications*, Nearfield Systems Inc., Torrance, CA, USA, 2004.
[22] F. Harrou and Y. Sun, "Statistical monitoring of linear antenna arrays," *Eng. Sci. Technol. Int. J.*, vol. 19, no. 4, pp. 1781–1787, 2016. [Online]. Available: https://www.sciencedirect.com/science/article/pii/S2215098616305900
[23] J. Fan, C. Zhang, and J. Zhang, "Generalized likelihood ratio statistics and Wilks phenomenon," *Ann. Statist.*, vol. 29, no. 1, pp. 153–193, 2001. [Online]. Available: https://doi.org/10.1214/aos/996986505
[24] D. Vakula and N. V. S. N. Sarma, "Using neural networks for fault detection in planar antenna arrays," *Progr. Electromagn. Res. Lett.*, vol. 14, pp. 21–30, Apr. 2010.
[25] D. Wang, D. Tan, and L. Liu, "Particle swarm optimization algorithm: An overview," *Soft Comput.*, vol. 22, no. 2, pp. 387–408, Jan. 2018. [Online]. Available: https://doi.org/10.1007/s00500-016-2474-6
[26] H. Al Kassir et al., "Improving DoA estimation via an optimal deep residual neural network classifier on uniform linear arrays," *IEEE Open J. Antennas Propag.*, vol. 5, pp. 460–473, 2024.
[27] Y. Fei, H. Cao, Y. Wu, X. Chen, and L. Chen, "DoA estimation in non-uniform noise using matrix completion via alternating projection," *IEEE Open J. Antennas Propag.*, vol. 2, pp. 281–285, 2021.
[28] V. Schenone, A. Fedeli, C. Estatico, M. Pastorino, and A. Randazzo, "Detection of failures in antenna arrays through a lebesgue-space approach," *IEEE Open J. Antennas Propag.*, vol. 3, pp. 652–662, 2022.
[29] S. Komeylian and C. Paolini, "Implementation of the digital QS-SVM-based beamformer on an FPGA platform," *Sensors*, vol. 23, no. 3, p. 1742, 2023.
[30] S. Komeylian, "Hybrid antenna array with the bowtie elements for super-resolution and 3D scanning radars," *Int. J. Electron. Commun. Eng.*, vol. 15, no. 1, pp. 54–59, 2014.
[31] S. Komeylian, A. Mihovska, M. Sarkar, and C. Paolini, "A FFNN-based system for the DoA estimation in 6G massive wireless communications: Analysis and evaluation," in *Proc. IEEE Wireless Commun. Netw. Conf.*, 2024, pp. 1–6.
[32] K. Huang and N. D. Sidiropoulos, "Consensus-ADMM for general quadratically constrained quadratic programming," *IEEE Trans. Signal Process.*, vol. 64, no. 20, pp. 5297–5310, Oct. 2016.
[33] Y. Zhang, E. Dall'Anese, and M. Hong, "Online proximal-ADMM for time-varying constrained convex optimization," *IEEE Trans. Signal Inf. Process. Over Netw.*, vol. 7, pp. 144–155, Feb. 2021, doi: 10.1109/TSIPN.2021.3051292.
[34] H. Tataria, P. J. Smith, L. J. Greenstein, P. A. Dmochowski, and M. Matthaiou, "Impact of line-of-sight and unequal spatial correlation on uplink MU-MIMO systems," *IEEE Wireless Commun. Lett.*, vol. 6, no. 5, pp. 634–637, Oct. 2017.
[35] S. Komeylian and C. Paolini, "Implementation of a three-class classification LS-SVM model for the hybrid antenna array with bowtie elements in the adaptive beamforming application," 2022, *arXiv:2210.00317*.
[36] J. A. Rodriguez-Gonzalez, F. Ares-Pena, M. Fernandez-Delgado, R. Iglesias, and S. Barro, "Rapid method for finding faulty elements in antenna arrays using far field pattern samples," *IEEE Trans. Antennas Propag.*, vol. 57, no. 6, pp. 1679–1683, Jun. 2009.